Unified Photocatalytic Strategy for the Cross-Coupling of Alcohols with Aryl Halides Enabled by Synergistic Nickel and Iron LMCT Catalysis

Mohammad Jaber, Yasemin Ozbay, Emmanuel Chefdeville, Gaël Tran, Abderrahmane Amgoune

A unified photocatalytic strategy for the cross coupling of alcohols with aryl halides enabled by synergistic nickel and iron LMCT catalysis

Mohammad Jaber,[†] Yasemin Ozbay,[†] Emmanuel Chefdeville,[‡] Gaël Tran,*[†] and Abderrahmane Amgoune*[,†,§]

† Université Lyon 1, Institut de Chimie et Biochimie Moléculaires et Supramoléculaires (ICBMS, UMR 5246 du CNRS), 1 rue Victor Grignard, 69100 Villeurbanne, France.

‡ Université Lyon 1, Centre Commun de Résonance Magnétique Nucléaire (CCRMN), 1 rue Victor Grignard, 69616 Villeurbanne, France.

§ Institut Universitaire de France (IUF), 1 rue Descartes, 75231 Paris, France.

KEYWORDS: Nickel catalysis – Iron catalysis – Native alcohols – Photoredox catalysis – Mechanistic studies

ABSTRACT: The use of alcohol feedstock as coupling partner in cross-coupling reactions offers an extraordinary potential for the efficient synthesis of Csp^3-rich complex molecular scaffolds. This prominent strategy relies on the generation of alkoxy radicals, which can react *via* various radical pathways to give carbon-centered radicals that can be engaged in C–C bond formation reactions. However, cross-coupling reactions involving catalytic generation of alkoxy radicals directly from native alcohols is highly challenging and the scope of existing catalytic methods remains particularly limited. Moreover, a unified strategy that can incorporate a broad range of alcohols in catalytic cross-coupling with aryl halides is currently unavailable. Herein, we report a general photocatalytic platform that combines nickel and iron ligand-to-metal charge transfer (LMCT) catalysis for the selective deconstructive Csp^3-Csp^3 bond cleavage and arylation of various unactivated alcohols. This protocol leverages the ability of photoinduced iron LMCT catalysis to generate radicals from diversely substituted alcohols, enabling implementation of various C–C bond-forming manifolds. These include dehydroxymethylative arylation of aliphatic alcohols, remote arylation of cyclic alcohols to yield alkyl ketones, and the methylation of aryl halides using tertiary alcohols as the methyl radical source. This methodology offers a practical and unified strategy for engaging a large variety of commercially available alcohols in cross-coupling reactions under mild conditions, using abundant nickel and iron catalysts. Mechanistic studies, including stoichiometric organometallic chemistry and cyclic voltammetry, provide insights into the crucial role of the ancillary ligand surrounding the iron catalyst in stabilizing both low- and high-valent iron catalytic intermediates.

1. Introduction

Bioactive compounds containing a high amount of Csp^3 centers tend to feature highly improved properties compared to more saturated analogues, *e.g.* better solubility profile or fewer off-target effects, resulting in improved pharmaco-kinetic and -dynamic profiles.[1] Recognizing this trend, the organic chemistry community has rapidly developed novel synthetic routes to sp^3-rich compounds. In particular, the renaissance of cross-couplings using first-row transition metal catalysts and the subsequent rise of metallaphotoredox catalysis have led to some of the most impactful methods in this field.[2] This radical-based approach has been so successful that a wide range of carbon radical precursors have been explored, including alkyl halides, silicates, trifluoroborates, carboxylates, redox-active esters or Katrizky salts.[3]

While these precursors cover significant chemical space, most are not "*native*" chemicals, reflected in their relatively low commercial availability and often cumbersome synthesis. In contrast, alcohols are ubiquitous both in natural and commercial sources and exhibit exceptional structural diversity, making them highly attractive as carbon-based radical precursors for cross-coupling reactions.[4] However, converting alcohols into carbon-based radicals is notoriously difficult, *typically requiring pre-activation of the alcohol* followed by homolytic cleavage of the resulting intermediate.[5] Although generally straightforward, these methods generate unnecessary waste, reducing the overall sustainability of the reaction and often limiting applicability to specific classes of alcohols.

Recent advances in modern photoredox strategies have enabled the catalytic generation of carbon-based radicals from free alcohols under mild conditions.[6] These strategies mainly rely on the photocatalytic formation of an alkoxy radical from the alcohol either via proton-coupled electron transfer (PCET) or ligand-to-metal charge transfer (LMCT) mechanisms, followed by transposition to carbon-based

radical (Figure 1). Despite these breakthroughs, the catalytic transformation of free alcohols into carbon-based radicals remains extremely rare within the context of metallaphotoredox catalysis, with only two notable examples to date. The group of Rueping achieved arylative ring opening reactions from cyclic alkanols bearing electron-rich aromatic cores by combining PCET catalysis with nickel catalysis.[7] Meanwhile, the group of Zuo employed a LMCT process from cerium complexes to develop a photocatalytic dehydroxymethylative arylation of primary aliphatic alcohols.[8,9] These elegant examples highlight the synthetic versatility

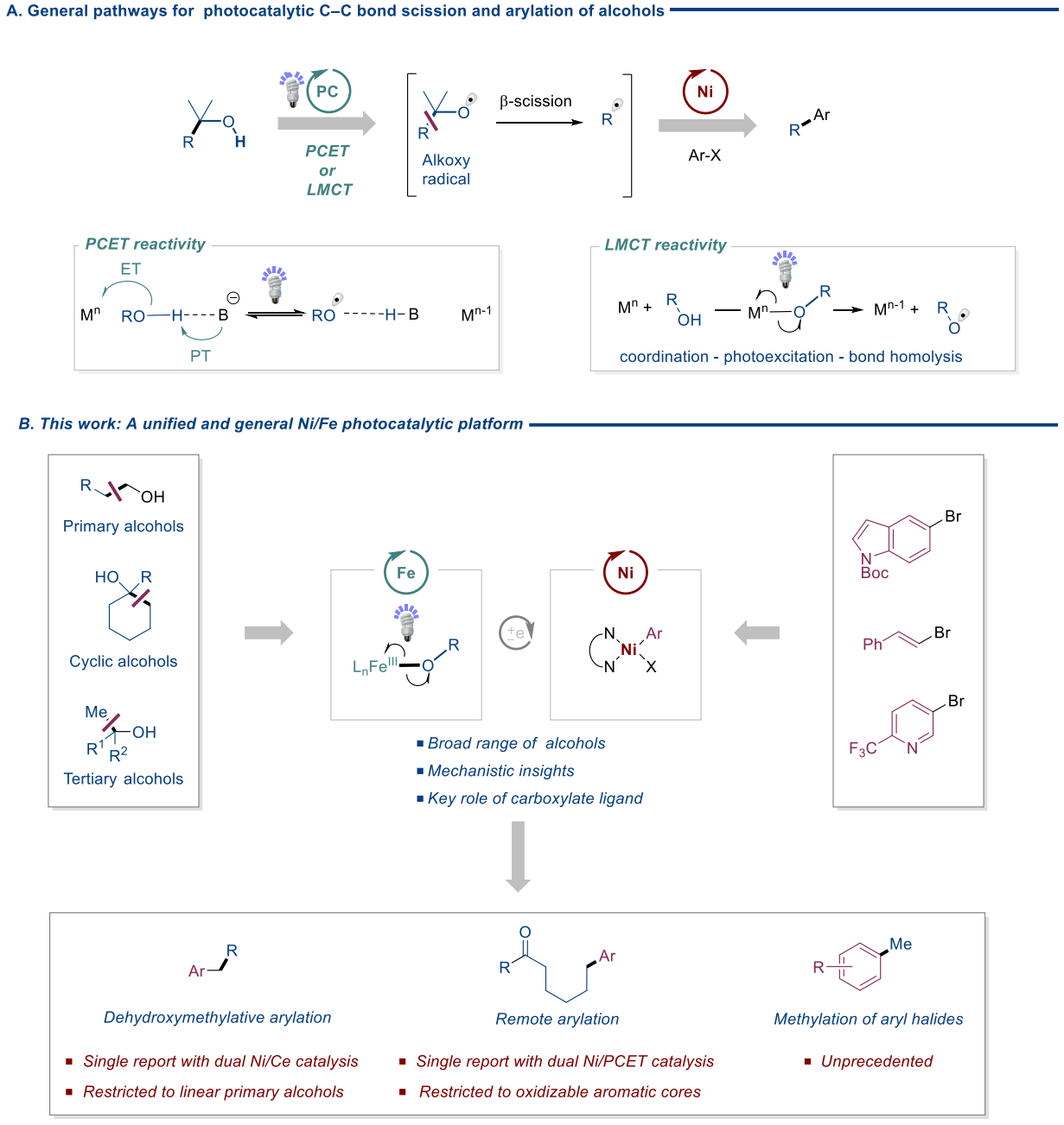

Figure 1. Cross-coupling reactions with native alcohols *via* radical C–C bond cleavage pathways (A) General pathway for catalytic transposition of alcohols to carbon-based radical *via* the PCET or LMCT strategy. (B) This work: A general protocol allowing the valorization of a broad range of alcohols.

offered by alkoxy radicals, as cycloalkanols lead to arylated ketones through C–C bond functionalization, whereas linear alcohols result in arylated alkyls through dehydroxymethylation. However, these protocols are limited to specific classes of alcohols. PCET activation is inherently restricted to oxidizable substrates, while LMCT from cerium complexes does not accommodate sterically hindered alcohols in this context. Considering the tremendous synthetic potential offered by implementing alkoxy radicals in nickel catalyzed radical cross-coupling reactions, we aimed to develop a general catalytic platform capable of coupling a broad range of alcohols. Achieving generality in metallaphotoredox catalysis is particularly challenging, as the intricate catalytic cycles must be kinetically matched to prevent the

accumulation and degradation of catalytic intermediates. In this perspective, we aimed to explore the photoinduced LMCT excitation strategy for several reasons: (*i*) LMCT catalysts are based on abundant and inexpensive transition metals such as copper, cerium, or iron, (*ii*) these catalysts operate through distinct photochemical pathways compared to commonly used photoredox catalysts. While the domain of photoredox catalysis is largely dominated by photocatalysts operating via outer-sphere single electron transfer processes, LMCT catalysts function through inner-sphere pathways.[10] Specifically, transition metals with LMCT excited states commonly undergo visible light-induced homolysis.[11] This mode of reactivity enables the transformation of nucleophilic entities into open-shell species *via* inner-sphere processes involving coordination of the substrate to the metal center, followed by photoinduced bond homolysis to generate a formally reduced metal center and a radical. This activation mode, proceeding through coordination chemistry, offers extensive opportunities to fine-tune the steric and electronic parameters governing the alcohol coordination and alkoxy radical generation steps. With these considerations in mind, we hypothesized that an effective LMCT catalyst should possess a low coordination number, allowing for the indiscriminate coordination of various types of alcohols. This feature would ensure continuous kinetic matching between catalytic cycles, even when the substrate classes change. We identified iron complexes as particularly promising due to their reported photoactivity in less crowded conformations.[12,13,14]

Herein we report a unified and practical photocatalytic strategy that enable various type of cross-coupling manifolds with primary and tertiary alcohols (Figure 1B). These include: *(i)* dehydroxymethylative arylation of aliphatic alcohols, *(ii)* remote arylation of cyclic alcohols to yield alkyl ketones, and *(iii)* the use of tertiary alcohols as methyl radical source for the methylation of aryl halides. The photocatalytic platform comprises a photoactive iron-LMCT catalyst capable of generating alkoxy radicals from a broad range of alcohols, and a nickel catalyst that promotes the oxidative addition of the aryl halide electrophilic partner, the capture of the alkyl radical and C–C bond formation. Catalytic turnover for both cycles is insured by an organophotoredox catalyst that acts as a redox shuttle between the two catalytic cycles. Mechanistic investigations have validated the role of each catalytic partner and provided key insights into the crucial role of the ancillary ligand surrounding the iron catalyst, which is essential for the efficient conversion of a broad range of alcohols.

2. Results and discussion

2.1. Optimization

Aryl bromide **1a** and alcohol **2a** were selected as model substrates for cross-coupling reactions using $FeCl_3$ as the LMCT catalyst, $NiCl_2$•DME/dMeBpy (**L$_{Ni1}$**) as the cross-coupling catalyst, 1,10-diphenylanthracene (DPA) photocatalyst as the electron shuttle between the [Fe] and [Ni] cycles, Na_3PO_4 as a base, in MeCN under 390 nm irradiation (Scheme 1). Initial attempts under these conditions yielded only trace amounts of the desired product, indicating inefficient alcohol activation. Given the significant impact of the iron coordination sphere on the efficiency of Fe(III) LMCT systems,[15] we decided to focus our attention on anionic ligands. Simple halides proved ineffective (<5% yield), but aryl carboxylates, formed in situ from the corresponding free acids, significantly improved the yield (Scheme 1A), achieving 30% yield with simple benzoic acid (**L$_{Fe1}$**). Further investigation of carboxylic acids with varying steric and electronic profiles led to the selection of the sterically hindered carboxylate **L$_{Fe9}$**, which afforded a 70% yield.

Numerous reaction parameters were systematically explored, but none had an impact as significant as the iron ligand (see supporting information for details). Ultimately, the following optimized conditions: $FeCl_2$ (10 mol%), **L$_{Fe9}$** (30 mol%), $NiCl_2$•DME/**L$_{Ni8}$** (2.5 mol%/3 mol%), DPA (2.5 mol%), and K_3PO_4 (3.0 eq) in MeCN under 390 nm irradiation, yielded product **3a** in 78% isolated yield.

Scheme 1. Ni/Fe catalyzed arylation of linear alcohols: selected optimization experiments.

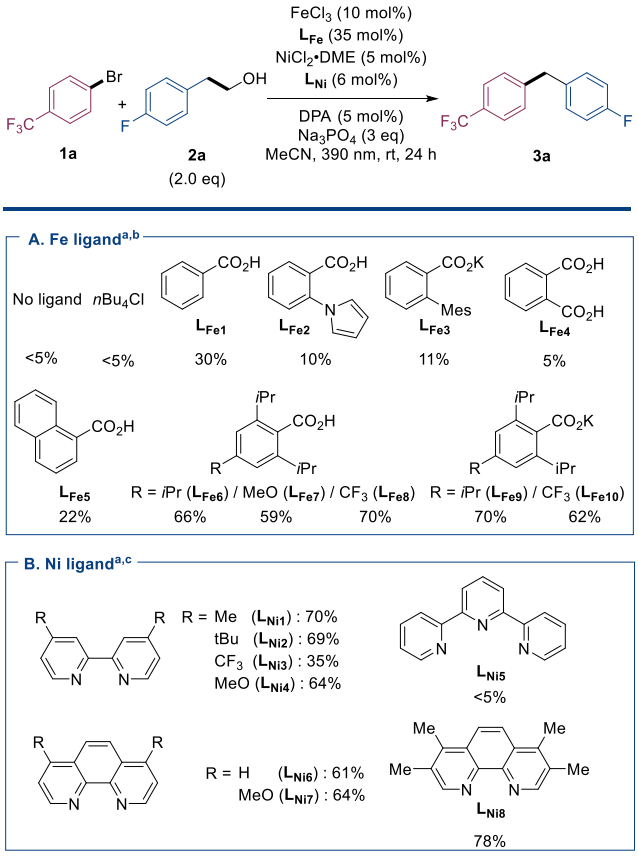

[a] Reactions performed on 0.20 mmol scale. Yields were determined by GCMS using $PhOCF_3$ as an internal standard. [b] **L$_{Ni}$ = L$_{Ni1}$** for the screening of Fe ligand [c] **L$_{Fe}$ = L$_{Fe9}$** for the screening of Ni ligands.

In addition to efficiently activating primary alcohols, we were pleased to find that this catalytic system also successfully enabled the cross-coupling of more sterically hindered tertiary cycloalkanols (Scheme 2). In contrast, a cerium LMCT catalyst failed to produce any trace of the desired

product under the same conditions, thereby supporting our initial hypothesis on the critical importance of the LMCT catalyst's low coordination number.

Scheme 2. Catalytic system efficiency with sterically hindered alcohols.

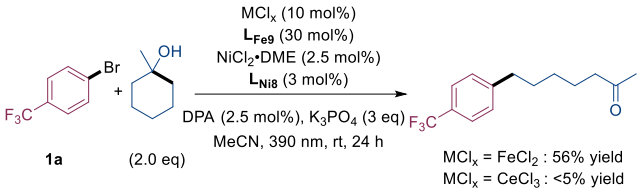

2.2. Scope and limitations

With the optimized conditions in hand, we first validated the ability of the Ni/Fe photocatalytic platform to enable the dehydroxymethylative arylation of aliphatic alcohols using a range of aryl bromides **1** and primary alcohols **2** (Table 1). Pleasingly, the reaction proceeded well with a broad tolerance to the electronic properties of the aryl bromide, yielding products in the range of 59% to 88% (**3-10**) irrespective of whether the aryl ring was electron-rich or electron-poor. Sensitive functionalities such as a cyano group (**4**, 88%) or a chlorine atom (**5**, 56%) were well tolerated. Significantly, biologically relevant heteroaryl bromides were compatible with the reaction (**11-14**), including strongly coordinating unsubstituted pyridine (**12**, 50%) and pyrimidine (**13**, 70%). Apart from aryl bromides, a vinyl bromide was also successfully engaged, yielding the desired product **15** with good efficiency, though with partial *E*/*Z* isomerization of the double bond. Regarding the alcohol scope, good to excellent yields were achieved with alcohols that form stabilized radicals, including benzylic alcohols (**16**), primary or secondary heteroatom-stabilized alcohols (**17-19**), and allylic alcohols (**20-21**). Unfortunately, primary alcohols leading to less stabilized radicals (*e.g.* 1-butanol, 2-cyclohexylethanol) gave strongly diminished yields (<20%).

Table 1. Scope for the dehydroxymethylative arylation of linear alcohols.[a]

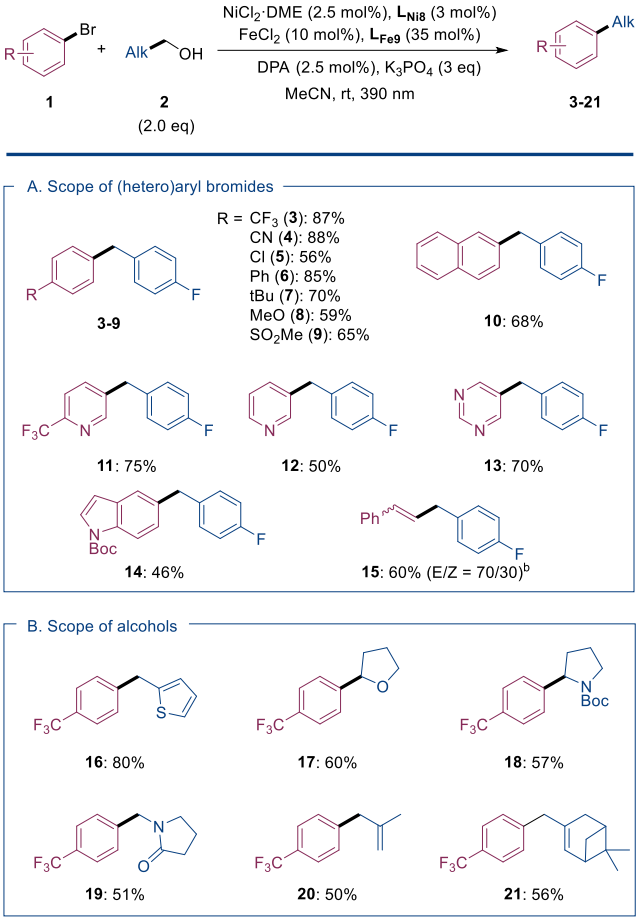

[a]Reactions performed on a 0.4 mmol scale. Isolated yields. [b]Determined by ^{1}H NMR.

Having demonstrated the efficient generation and coupling of carbon-based radicals from primary alcohols in the dehydroxymethylative arylation protocol, we next focused on the more challenging sterically hindered cycloalkanols (Table 2A). Activating C–C bonds in this widely available substrate family is highly desirable as it provides a direct route to remotely arylated ketones. However, the difficulty associated with activating these substrates has made this transformation elusive, typically limited to cycloalkanols with oxidizable aromatic rings.[7] Therefore, we were pleased to find that cycloalkanols of various ring sizes yielded the corresponding ketones (**22-25**) in good to excellent yields. Additionally, heteroatom-containing and benzo-fused cycloalkanols proved to be suitable substrates, enabling the synthesis of complex ketones (**26-28**), and the use of cycloakanols bearing a phenyl substituent (**29**) or a longer alkyl chain substituent (**30**) was tolerated as well. Similarly to the dehydroxymethylative arylation, this remote arylation protocol exhibited excellent functional group compatibility, accommodating electron-withdrawing and electron-donating groups, as well as sensitive functionalities and nitrogen-containing heterocycles (**31-38**). Importantly, high selectivity of the *β*-scission toward ring opening was observed in all cases, with only minutes amounts of by-products originating from alternative *β*-scission sites. In terms of limitations, secondary cyclic alcohols systematically led to low yields. Encouraged by these results, we explored whether acyclic tertiary alcohols could also serve as radical sources (Table

2B). We hypothesized that both enthalpic factors (*i.e.*, formation of a substituted C=O bond) and entropic factors (*i.e.*, increased conformational freedom) would be preserved between cycloalkanols and acyclic alcohols, making the reaction thermodynamically feasible. This transformation would be highly significant, enabling the generation of unstabilized radicals from readily available, non-toxic reagents. In particular, achieving the challenging methylative cross-coupling would be exceptionally impactful due to its broad utility in the synthesis of bioactive molecules.[16] Despite being a very active research area, current methylation protocols are often hampered by issues of toxicity, functional group compatibility, and atom efficiency.[17] Given these considerations, we tested the simplest tertiary alcohol, *tert*-butanol, under our benchmark conditions, which unfortunately resulted in low yields (34%). However, the inexpensive, non-toxic, and easy-to-handle α-cumyl alcohol proved to be much more efficient, yielding the corresponding methylated products in good to average yields (**39-47**). The reaction again showed tolerance for sensitive functionalities, such as -BPin or -SO_2Me groups (**41-42**), and biologically relevant heterocycles (**43-46**). Additionally, other unstabilized alkyl radicals were selectively generated, as demonstrated by the incorporation of a cyclohexyl moiety (**47**). However, tertiary alkyl radicals did not lead to significant amounts of cross-coupling, which is a classical limitation of nickel/photoredox manifolds.[18]

Table 2. Scope for the arylation with tertiary alcohols.

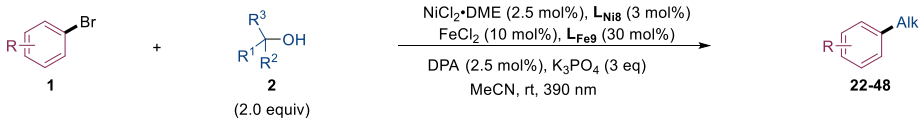

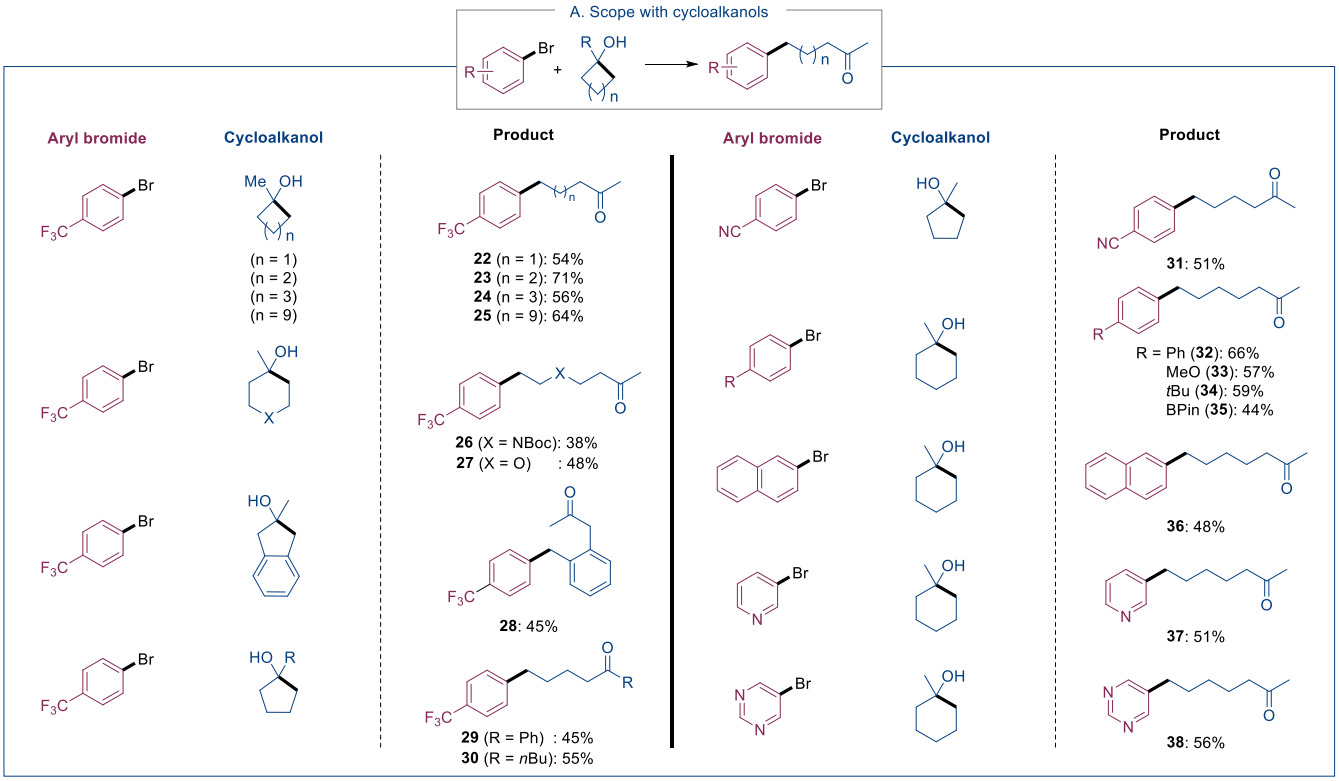

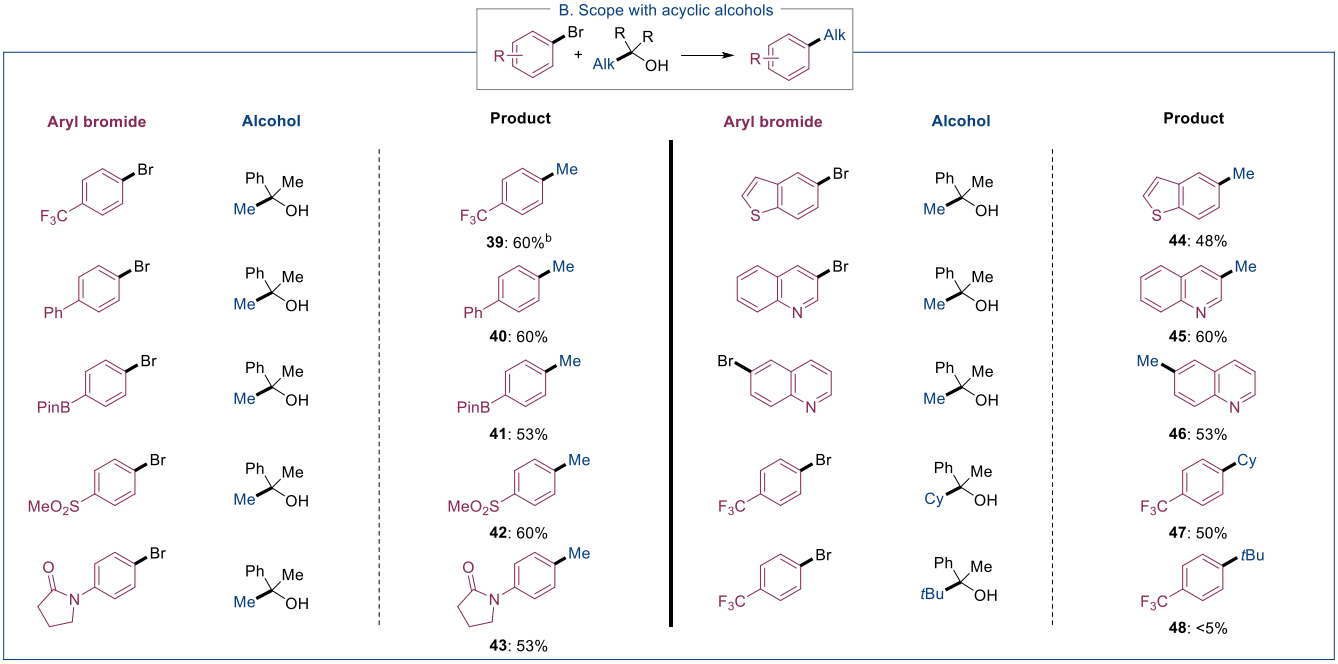

[a] Reactions performed on a 0.4 mmol scale. Isolated yields. [b] Yields determined by ^{1}H or ^{19}F NMR.

2.3. Mechanistic investigations

As previously underlined, very few dual-catalyzed methods involving LMCT activation of metal-alkoxides have been de-

scribed to date.[8,9,14] Consequently, the parameters governing the reactivity and the mechanistic subtleties of this class of reactions remain essentially unknown, thus hampering its broader application to unexplored substrate classes. Key mechanistic questions include the role of the iron coordination sphere and the actual involvement of iron alkoxide within the catalytic cycle. To provide some mechanistic insights, we conducted a series of cyclic voltammetry (CV) studies and stoichiometric experiments.

We first sought to analyze the influence of the carboxylate ligand on the redox behavior of iron species. To this end, we examined the cyclic voltammogram of $FeCl_2$ in MeCN (0.1 M $TBAPF_6$; GC WE; Pt CE; $Ag/AgNO_3$ ref), in the absence and presence of the carboxylate ligand $\mathbf{L_{Fe9}}$ (Figure 2A, left). Upon anodic scanning, the CV of $FeCl_2$ exhibited a broad quasi-reversible oxidation peak (O_1 = +0.01 V; R_1 = -0.10 V) corresponding to the Fe(II)/Fe(III) couple, along with several irreversible reduction peaks at lower potentials (R_2 = -1.24 V; R_3 = -1.62 V). The shape of these latter peaks is characteristic of electrodeposition, presumably of Fe(0) films,[19] and was associated with an intense stripping peak upon reverse oxidative scanning (O_2). The addition of 3 eq of $\mathbf{L_{Fe9}}$ to this solution led to a marked cathodic shift of the Fe(II) to Fe(III) oxidation (O'_1 = -0.08 V) and a loss of reversibility of the Fe(II)/Fe(III) couple. Specifically, the return reduction peak R'_1 was considerably broadened and dramatically shifted to -1.08 V, suggesting an evolution of the iron coordination sphere upon oxidation. Notably, the newly formed species did not display any additional reduction peaks until -2.05 V (R'_2).

Next, we examined the effect of alcohol **2a** and K_3PO_4 on these solutions. For $FeCl_2$ (Figure 2A, middle), no significant change was observed in the Fe(II)/Fe(III) redox peaks O''_1 and R"1. Reduction to low valent iron remained observable at relatively high potential (R''_2 = -1.43 V). In contrast, the addition of **2a** and K_3PO_4 to the solution of $FeCl_2$ and $\mathbf{L_{Fe9}}$ resulted in significant modifications in the cyclic voltammogram (Figure 2A, right). The Fe(II) to Fe(III) oxidation peak was anodically shifted (O'''_1 = +0.34 V), the return wave was cathodically shifted (R'''_1 = -1.60 V) and other reductive features at lower potential disappeared.

These observations highlight three beneficial effects of $\mathbf{L_{Fe9}}$ on the iron catalytic system: (*i*) it provides enhanced stability to Fe(III) species, as evidenced by the large cathodic shift of the Fe(III) reduction peak R'_1; (*ii*) it protects low valent iron species from degradation to Fe(0) particles by shifting the corresponding reductive waves outside of the reduction range of the photocatalyst; (*iii*) it enhances interaction of iron complexes with alcohols, as suggested by the shifts in the redox waves in the presence of alcohol.

While these experiments demonstrate the ability of carboxylate $\mathbf{L_{Fe9}}$ to interact with $FeCl_2$ and highlight its potential impact on catalytic efficiency, the precise nature of the resulting species remains unclear. To get further structural insights, we attempted to isolate and characterize the iron carboxylate species formed from the reaction of $FeCl_2$ with various amounts of $\mathbf{L_{Fe9}}$ (1 to 3 eq).[20] Although copious amounts of chloride salts precipitated in all cases, the 1:2 $FeCl_2$/$\mathbf{L_{Fe9}}$ mixture successfully yielded X-Ray suitable crystals (Figure 2B). The molecular structure of **I** is composed of an oxo-bridged Fe_3O trimer core,[21] which is surrounded by six bridging carboxylates and three acetonitrile molecules. Thus, each iron center sits in octahedral coordination geometry. Overall, the trimer complex closely resembles previously reported Fe^{III}-Fe^{III}-Fe^{II} mixed-valence complex.[22] The Fe atoms in **I** featured two distinct sets of bond lengths with surrounding atoms, consistent with the ranges observed in related complexes.[22]

Interestingly, independent analysis of complex **I** by ^{1}H NMR and cyclic voltammetry revealed similar features than species formed *in-situ* by mixing $FeCl_2$ and 2 eq of $\mathbf{L_{Fe9}}$ (Figure 2C and 2D). However, introducing an additional equivalent of $\mathbf{L_{Fe9}}$ led to significant spectral differences compared to **I**, suggesting that trimeric structures like **I** evolve further in solution when 3 eq of $\mathbf{L_{Fe9}}$ are present. Addition of alcohol **2a** and K_3PO_4 to **I** led to strong shift of the paramagnetic signals in ^{1}H NMR, as well as a shift of the protons in α position of the alcohol ($\Delta\delta$ = 0.45ppm).

To further probe the nature of these complexes, we conducted a set of DOSY NMR experiments on catalytically relevant complexes (see spectra in Supporting Information). While DOSY is commonly used to evaluate the size of diamagnetic organometallic complexes,[23] characterizing paramagnetic complexes is significantly more challenging due to peak broadness and rapid T1 relaxation.[24] Nevertheless, we successfully obtained exploitable signals, presenting rare results from paramagnetic DOSY experiments. First, complex **I** showed a low diffusion coefficient D = 8.65 x 10^{-10} m^2/s, corresponding to a hydrodynamic radius r_H of 7.03 Å. This result is consistent with the diameter of complex **I** (14.4 Å), as determined from the X-Ray structure. This experiment not only demonstrates that complex **I** retains an oligomeric structure in solution but also serves as a useful benchmark for evaluating the nuclearity of other in-situ generated complexes. For instance, the species formed *in-situ* from FeCl2 + 3 eq $\mathbf{L_{Fe9}}$ also exhibited a low diffusion coefficient D = 6.6 x 10^{-10} m^2/s, corresponding to a hydrodynamic radius r_H of 9.21 Å, consistent with retention of an oligomeric structure. Finally, DOSY analysis of a mixture of FeCl2 + 3 eq $\mathbf{L_{Fe9}}$ + 5 eq of alcohol **2a** + 7.5 eq K_3PO_4 revealed signals attributable to **2a** with a diffusion coefficient D = 1.85 x 10^{-9} m^2/s. Crucially, this coefficient is significantly lower than that of the free alcohol (D = 2.70 x 10^{-9} m^2/s), providing clear evidence of alcohol interaction with a much larger molecule.

To consolidate the relevance of these complexes, the ability of complex **I** to generate alkoxy radicals from alcohol was confirmed by reaction with **2a** in the presence of K_3PO_4 and $\mathbf{L_{Fe9}}$ under irradiation, resulting in good yields of the corresponding dimer (calculated *vs* the number of Fe atoms, Figure 2E). Complex **I** was also shown to be catalytically active, although with decreased yields compared to the benchmark conditions. However, similar yields were observed upon the addition of 10 mol% of $\mathbf{L_{Fe9}}$ (Figure 2F, entries 1 and 2). Furthermore, complex **I** demonstrated catalytic activity in the complete absence of chloride anions (Figure 2F entry 3), which further support the involvement of iron alkoxide as the LMCT-active species.[25]

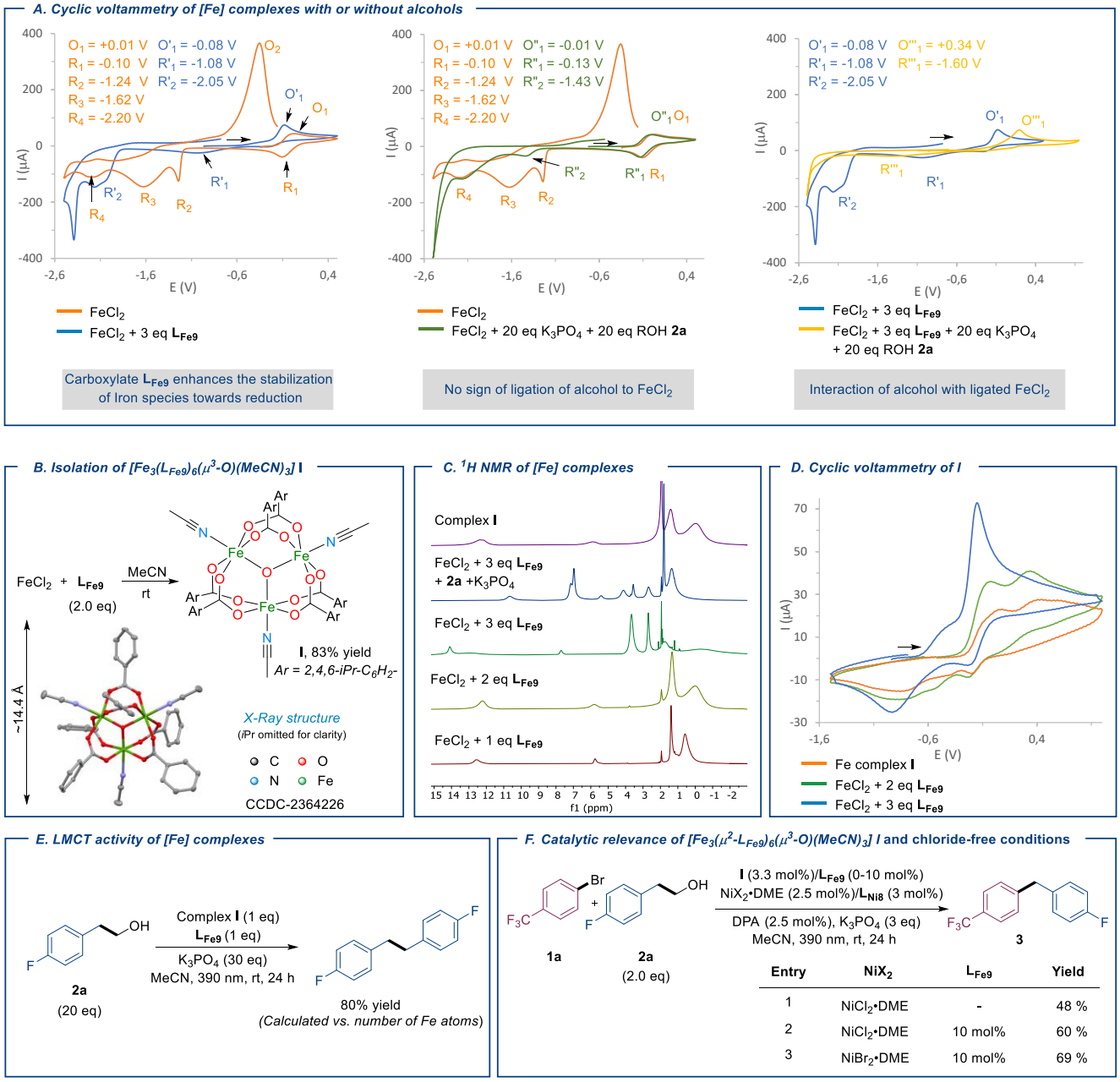

Figure 2. Mechanistic investigations into the iron catalytic cycle. (A) Cyclic voltammetry of differently ligated $FeCl_2$; (B) Synthesis and isolation of oxo-bridged trimer **I**; (C) ^{1}H NMR analysis of [Fe] complexes; (D) Comparison of cyclic voltammetry of **I** and of *in-situ* formed complexes; (E) Stoichiometric LMCT activity of **I**; (F) Catalytic relevance of **I** and chloride-free conditions.

Having clarified the behavior of the iron catalytic cycle, we turned our attention to the nickel catalytic cycle. First, we recorded the cyclic voltammogram of ($\mathbf{L_{Ni8}}$)$NiCl_2$ (formed *in-situ* from $NiCl_2$•DME and $\mathbf{L_{Ni8}}$) (Figure 3A and Figure S9). Upon cathodic scanning, two well-defined reduction waves R_1 (-1.39 V) and R_2 (-1.82 V) were observed, each associated with a main return wave, O_1 (-0.19 V) and O_2 (-1.12 V), respectively. When aryl bromide **1a** (5 eq) is added to the 1:1 mixture of $NiCl_2$•DME/$\mathbf{L_{Ni8}}$ an increase of the current is observed at the second reduction peak R'_2, along with the loss of the return oxidation peak O_2 (Figure 3A). Intriguingly, the first reduction peak R'_1 and the associated return oxidation peak O'_1 remained unchanged. This indicates that the species associated with R'_2 do not originate from R'_1 (*e.g.* Ni^{II}/Ni^{I} reduction followed by Ni^{I}/Ni^{0} reduction). Instead, R'_2 and R'_1 were attributed to the reduction of two differently speciated Ni^{II} species.[26] Although the exact nature of these species and the number of electrons associated with R'_1 and R'_2 remain to be clarified, the magnitude of the current increase between R_2 and R'_2 (from -103 µA to -260 µA) is consistent with an initial one electron reduction from Ni^{II} to Ni^{I} followed by oxidative addition to Ni^{III} and subsequent two electrons reduction to Ni^{I} (Figure 3A). Moreover, a new

return oxidation wave O'$_3$ was also observed at (-0.19 V), suggesting the oxidation of new nickel species.

To gain further insights into the formation and electrochemical behavior of nickel intermediates resulting from the addition of ArBr to the 1:1 mixture of $NiCl_2$.DME/$\mathbf{L_{Ni8}}$, we independently prepared the corresponding oxidative addition complex **II** (Figure 3B). The cyclic voltammogram of complex **II** displays a reduction peak at -1.48 V and a return oxidation wave at +0.20 V that compares well with the oxidation peak O'$_3$. This corroborates that the oxidative addition complex **II** is formed as an intermediate upon electroreduction of $NiCl_2$•DME/$\mathbf{L_{Ni8}}$ in the presence of aryl bromide **1a**. Furthermore, we confirmed that complex **II** is able to intercept carbon-based radicals generated from Fe-LMCT, thus leading to cross-coupled product **3** in 57% yield, and that it is a catalytically active species under standard reaction conditions (Figure 3B).

Taken together, the above experiments support the catalytic cycle depicted in Figure 4. First, a carboxylate-ligated Fe^{II} complex **A** (E^{p}_{ox} = -0.08 V) gets oxidized by DPA* ($E^{1/2}$(DPA*/DPA) = +0.95 V *vs.* Ag/$AgNO_3$)[27] to Fe^{III} complex **B**, followed by alcohol complexation.[28] The ensuing species **C** can then undergo LMCT excitation, resulting in Fe^{III}-O bond homolysis and regeneration of **A**. The nickel catalytic cycle is initiated from a Ni^{I} complex **E**, which undergoes oxidative addition with ArBr to give high-valent Ni^{III} complex **F**, which is immediately reduced to Ni^{II} **G** (E^{p}_{ox}(G/F) = +0.20 V) by DPA$^{-\bullet}$ ($E^{1/2}$(DPA/DPA$^{-\bullet}$) = -2.24 V).[29] Capture of radical R$^{\bullet}$ by **G** and reductive elimination complete the catalytic cycle.

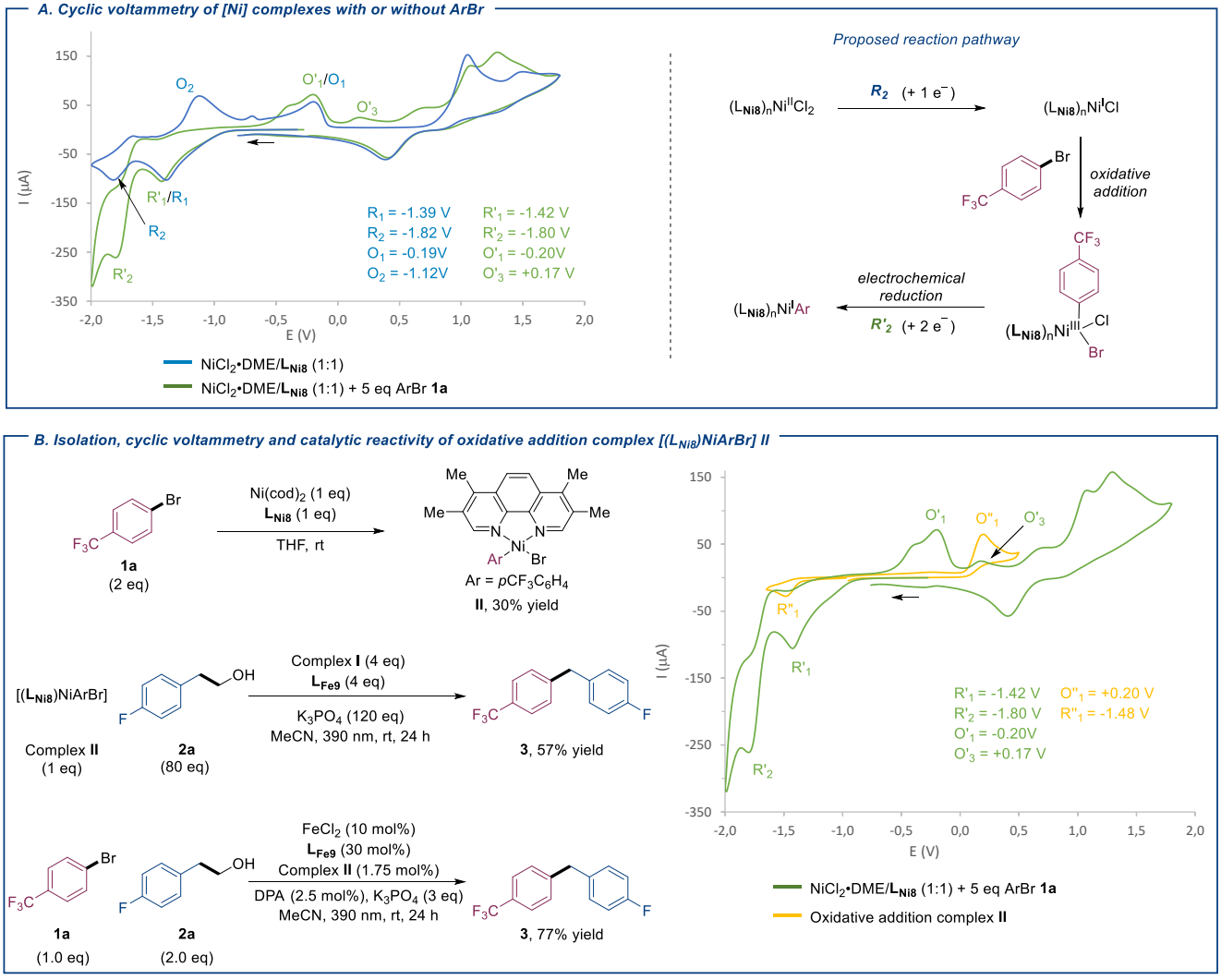

Figure 3. Mechanistic investigations into the nickel catalytic cycle. (A) Cyclic voltammetry of $NiCl_2$•DME/$\mathbf{L_{Ni8}}$ (1:1) with and without ArBr (left), and proposed reaction pathway (right); (B) Isolation (upper left), catalytic relevance (lower left) cyclic voltammetry (right) of oxidative addition complex **II**.

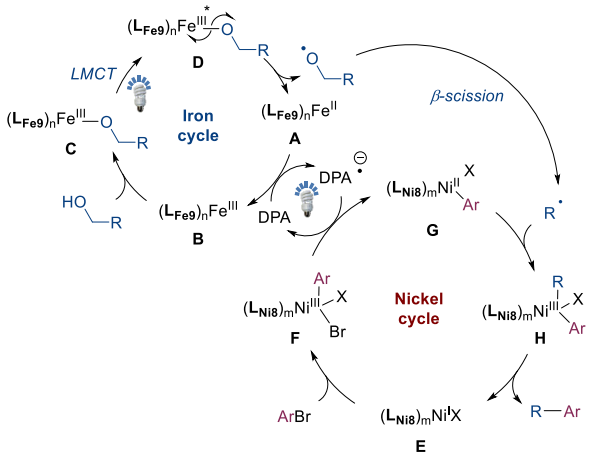

Figure 4. Proposed catalytic pathway

3. Conclusions

In summary, we have developed a versatile cross-coupling methodology between a wide range of commercially available alcohols and Csp^2-halides under mild conditions, using abundant nickel and iron catalysts. This unified strategy enables various transformations: *(i)* dehydroxymethylative arylation of aliphatic alcohols, *(ii)* remote arylation of cyclic alcohols to yield alkyl ketones, and *(iii)* the use of tertiary alcohols as methyl radical source for the methylation of aryl halides. From a broader perspective, this work showcases the efficient implementation of iron LMCT catalysis in the area of nickel/photoredox catalysis, thereby expanding the mechanistic landscape of cross-coupling reactions. Mechanistic studies have shed light on key features of this catalytic system, particularly the role of carboxylate ligands in stabilizing both low- and high-valent iron catalytic species against undesired reduction, thereby favoring the desired [Fe^{III}-OR] LMCT pathway. This key insight should prove decisive in the future development of related dual catalytic systems. Overall, this work paves the way for a large application of dual catalytic systems involving LMCT activation of alcohols, a field of tremendous potential poised to unlock vast areas of chemical space.

MATERIALS AND METHODS

All details pertaining to materials and methods are reported in the supporting information.

AUTHOR INFORMATION

Corresponding Authors

*Gaël Tran: gael.tran@univ-lyon1.fr – ORCID: 0000-0001-7817-5255

*Abderrahmane Amgoune: abderrahmane.amgoune@univ-lyon1.fr – ORCID: 0000-0002-6195-1411

Authors

Mohammad Jaber

Yasemin Ozbay

Emmanuel Chefdeville

Author Contributions

The manuscript was written through contributions of all authors. All authors have given approval to the final version of the manuscript.

ASSOCIATED CONTENT

Supporting Information

The Supporting Information is available free of charge on the ACS Publications website.

The Supporting Information contains experimental procedures and graphical abstracts for the reaction, investigation of the reaction parameters, optimization of the reaction conditions, mechanistic experiments, analysis, and compound characterization data.

ACKNOWLEDGMENT

This work was supported by the CNRS, the French Ministry of Research, the ICBMS and the Université Claude Bernard Lyon 1. Financial support from the Agence Nationale de la Recherche (ANR-21-CE07-0022-01 NICECAT) is gratefully acknowledged. The NMR and Mass Centres of the Université Claude Bernard Lyon 1 are thanked for their contribution. A. A. thanks the Institut Universitaire de France (IUF) for its support. We thank Maurice Médebielle for his help with cyclic voltammetry experiments.

REFERENCES

(1) a) Lovering, F.; Bikker, J.; Humblet, C. Escape from Flatland: Increasing Saturation as an Approach to Improving Clinical Success. *J. Med. Chem.* **2009**, *52* (21), 6752–6756. b) Lovering, F. Escape from Flatland 2: Complexity and Promiscuity. *Med. Chem. Commun.* **2013**, *4* (3), 515–519.

(2) a) Chan, A. Y.; Perry, I. B.; Bissonnette, N. B.; Buksh, B. F.; Edwards, G. A.; Frye, L. I.; Garry, O. L.; Lavagnino, M. N.; Li, B. X.; Liang, Y.; Mao, E.; Millet, A.; Oakley, J. V.; Reed, N. L.; Sakai, H. A.; Seath, C. P.; MacMillan, D. W. C. Metallaphotoredox: The Merger of Photoredox and Transition Metal Catalysis. *Chem. Rev*. **2022**, *122* (2), 1485–1542. b) Zhang, J.; Rueping, M. Metallaphotoredox Catalysis for sp^3 C–H Functionalizations through Hydrogen Atom Transfer (HAT). *Chem. Soc. Rev.* **2023**, *52* (12), 4099–4120.

(3) For selected examples, see: a) Weix, D. J. Methods and Mechanisms for Cross-Electrophile Coupling of Csp^2 Halides with Alkyl Electrophiles. *Acc. Chem. Res.* **2015**, *48* (6), 1767–1775. b) Zhang, P.; Le, C. "Chip"; MacMillan, D. W. C. Silyl Radical Activation of Alkyl Halides in Metallaphotoredox Catalysis: A Unique Pathway for Cross-Electrophile Coupling. *J. Am. Chem. Soc.* **2016**, *138* (26), 8084–8087. c) Lévêque, C.; Chenneberg, L.; Corcé, V.; Goddard, J.-P.; Ollivier, C.; Fensterbank, L. Primary Alkyl Bis-Catecholato Silicates in Dual Photoredox/Nickel Catalysis: Aryl- and Heteroaryl-Alkyl Cross Coupling Reactions. *Org. Chem. Front.* **2016**, *3* (4), 462–465. d) Jouffroy, M.; Primer, D. N.; Molander, G. A. Base-Free Photoredox/Nickel Dual-Catalytic Cross-Coupling of Ammonium Alkylsilicates. *J. Am. Chem. Soc.* **2016**, *138* (2), 475–478. e) Zuo, Z.; Ahneman, D. T.; Chu, L.; Terrett, J. A.; Doyle, A. G.; MacMillan, D. W. C. Merging Photoredox with Nickel Catalysis: Coupling of α-Carboxyl sp^3-Carbons with Aryl Halides. *Science* **2014**, *345* (6195), 437–440. f) Cornella, J.; Edwards, J. T.; Qin, T.; Kawamura, S.; Wang, J.; Pan, C.-M.; Gianatassio, R.; Schmidt, M.; Eastgate, M. D.; Baran, P. S. Practical Ni-Catalyzed Aryl–Alkyl Cross-Coupling of Secondary Redox-Active Esters. *J. Am. Chem. Soc.* **2016**, *138* (7), 2174–2177. g) Turro, R. F.; Wahlman, J. L. H.; Tong, Z. J.; Chen, X.; Yang,

M.; Chen, E. P.; Hong, X.; Hadt, R. G.; Houk, K. N.; Yang, Y.-F.; Reisman, S. E. Mechanistic Investigation of Ni-Catalyzed Reductive Cross-Coupling of Alkenyl and Benzyl Electrophiles. *J. Am. Chem. Soc.* **2023**, *145* (27), 14705–14715. h) Huihui, K. M. M.; Caputo, J. A.; Melchor, Z.; Olivares, A. M.; Spiewak, A. M.; Johnson, K. A.; DiBenedetto, T. A.; Kim, S.; Ackerman, L. K. G.; Weix, D. J. Decarboxylative Cross-Electrophile Coupling of N-Hydroxyphthalimide Esters with Aryl Iodides. *J. Am. Chem. Soc.* **2016**, *138* (15), 5016–5019. i) Martin-Montero, R.; Yatham, V. R.; Yin, H.; Davies, J.; Martin, R. Ni-Catalyzed Reductive Deaminative Arylation at sp^3 Carbon Centers. *Org. Lett.* **2019**, *21* (8), 2947–2951. j) Plunkett, S.; Basch, C. H.; Santana, S. O.; Watson, M. P. Harnessing Alkylpyridinium Salts as Electrophiles in Deaminative Alkyl–Alkyl Cross-Couplings. *J. Am. Chem. Soc.* **2019**, *141* (6), 2257–2262.

(4) a) Ertl, P.; Schuhmann, T. A Systematic Cheminformatics Analysis of Functional Groups Occurring in Natural Products. *J. Nat. Prod.* **2019**, *82* (5), 1258–1263. b) Henkel, T.; Brunne, R. M.; Müller, H.; Reichel, F. Statistical Investigation into the Structural Complementarity of Natural Products and Synthetic Compounds. *Angew. Chem. Int. Ed.* **1999**, *38* (5), 643–647.

(5) For selected examples, see : a) Barton, D. H. R.; McCombie, S. W. A New Method for the Deoxygenation of Secondary Alcohols. *J. Chem. Soc., Perkin Trans. 1* **1975**, No. 16, 1574–1585. b) Lopez, R. M.; Hays, D. S.; Fu, G. C. Bu_3SnH-Catalyzed Barton–McCombie Deoxygenation of Alcohols. *J. Am. Chem. Soc.* **1997**, *119* (29), 6949–6950. c) Chenneberg, L.; Baralle, A.; Daniel, M.; Fensterbank, L.; Goddard, J.-P.; Ollivier, C. Visible Light Photocatalytic Reduction of O-Thiocarbamates: Development of a Tin-Free Barton–McCombie Deoxygenation Reaction. *Adv. Synth. Catal.* **2014**, *356* (13), 2756–2762. d) Friese, F. W.; Studer, A. Deoxygenative Borylation of Secondary and Tertiary Alcohols. *Angew. Chem. Int. Ed.* **2019**, *58* (28), 9561–9564. e) Wu, J.; Bär, R. M.; Guo, L.; Noble, A.; Aggarwal, V. K. Photoinduced Deoxygenative Borylations of Aliphatic Alcohols. *Angew. Chem. Int. Ed.* **2019**, *58* (52), 18830–18834. f) Zhang, L.; Koreeda, M. Radical Deoxygenation of Hydroxyl Groups via Phosphites. *J. Am. Chem. Soc.* **2004**, *126* (41), 13190–13191. g) Li, Z.; Sun, W.; Wang, X.; Li, L.; Zhang, Y.; Li, C. Electrochemically Enabled, Nickel-Catalyzed Dehydroxylative Cross-Coupling of Alcohols with Aryl Halides. *J. Am. Chem. Soc.* **2021**, *143* (9), 3536–3543. h) Guo, P.; Wang, K.; Jin, W.-J.; Xie, H.; Qi, L.; Liu, X.-Y.; Shu, X.-Z. Dynamic Kinetic Cross-Electrophile Arylation of Benzyl Alcohols by Nickel Catalysis. *J. Am. Chem. Soc.* **2021**, *143* (1), 513–523. i) Suga, T.; Ukaji, Y. Nickel-Catalyzed Cross-Electrophile Coupling between Benzyl Alcohols and Aryl Halides Assisted by Titanium Co-Reductant. *Org. Lett.* **2018**, *20* (24), 7846–7850. j) Jia, X.-G.; Guo, P.; Duan, J.; Shu, X.-Z. Dual Nickel and Lewis Acid Catalysis for Cross-Electrophile Coupling: The Allylation of Aryl Halides with Allylic Alcohols. *Chem. Sci.* **2018**, *9* (3), 640–645. k) Cong, F.; Lv, X.-Y.; Day, C. S.; Martin, R. Dual Catalytic Strategy for Forging sp^2–sp^3 and sp^3–sp^3 Architectures via β-Scission of Aliphatic Alcohol Derivatives. *J. Am. Chem. Soc.* **2020**, *142* (49), 20594–20599. l) Dong, Z.; MacMillan, D. W. C. Metallaphotoredox-Enabled Deoxygenative Arylation of Alcohols. *Nature* **2021**, *598* (7881), 451–456.

(6) a) Tsui, E.; Wang, H.; Knowles, R. R. Catalytic Generation of Alkoxy Radicals from Unfunctionalized Alcohols. *Chem. Sci.* **2020**, *11* (41), 11124–11141. b) Chang, L.; An, Q.; Duan, L.; Feng, K.; Zuo, Z. Alkoxy Radicals See the Light: New Paradigms of Photochemical Synthesis. *Chem. Rev.* **2022**, *122* (2), 2429–2486.

(7) Huang, L.; Ji, T.; Rueping, M. Remote Nickel-Catalyzed Cross-Coupling Arylation via Proton-Coupled Electron Transfer-Enabled C–C Bond Cleavage. *J. Am. Chem. Soc.* **2020**, *142* (7), 3532–3539.

(8) Chen, Y.; Wang, X.; He, X.; An, Q.; Zuo, Z. Photocatalytic Dehydroxymethylative Arylation by Synergistic Cerium and Nickel Catalysis. *J. Am. Chem. Soc.* **2021**, *143* (13), 4896–4902.

(9) For other seminal work on Ce-LMCT of alcohols, see: a) Guo, J.-J.; Hu, A.; Chen, Y.; Sun, J.; Tang, H.; Zuo, Z. Photocatalytic C–C Bond Cleavage and Amination of Cycloalkanols by Cerium(III) Chloride Complex. *Angew. Chem. Int. Ed.* **2016**, *55* (49), 15319–15322. b) Hu, A.; Guo, J.-J.; Pan, H.; Zuo, Z. Selective Functionalization of Methane, Ethane, and Higher Alkanes by Cerium Photocatalysis. *Science* **2018**, *361* (6403), 668–672. c) Hu, A.; Guo, J.-J.; Pan, H.; Tang, H.; Gao, Z.; Zuo, Z. δ-Selective Functionalization of Alkanols Enabled by Visible-Light-Induced Ligand-to-Metal Charge Transfer. *J. Am. Chem. Soc.* **2018**, *140* (5), 1612–1616. d) Zhang, K.; Chang, L.; An, Q.; Wang, X.; Zuo, Z. Dehydroxymethylation of Alcohols Enabled by Cerium Photocatalysis. *J. Am. Chem. Soc.* **2019**, *141* (26), 10556–10564. e) Schwarz, J. ; König, B. Visible-light mediated C–C bond cleavage of 1,2-diols to carbonyls by cerium-photocatalysis *Chem. Commun.* **2019**, *55*, 486–488.

(10) a) May, A. M.; Dempsey, J. L. A New Era of LMCT: Leveraging Ligand-to-Metal Charge Transfer Excited States for Photochemical Reactions. *Chem. Sci.* **2024**, *15* (18), 6661–6678. b) Juliá, F. Ligand-to-Metal Charge Transfer (LMCT) Photochemistry at 3d-Metal Complexes: An Emerging Tool for Sustainable Organic Synthesis. *ChemCatChem* **2022**, *14* (19), e202200916.

(11) Abderrazak, Y.; Bhattacharyya, A.; Reiser, O. Visible-Light-Induced Homolysis of Earth-Abundant Metal-Substrate Complexes: A Complementary Activation Strategy in Photoredox Catalysis. *Angew. Chem. Int. Ed.* **2021**, *60* (39), 21100–21115.

(12) For reported examples of alcohols activation involving Fe LMCT, see a) Reichgott, D. W.; Rose, N. J. Photoassisted Oxidation of Methanol Catalyzed by a Macrocyclic Iron Complex. *J. Am. Chem. Soc.* **1977**, *99* (6), 1813–1818. b) Liu, W.; Wu, Q.; Wang, M.; Huang, Y.; Hu, P. Iron-Catalyzed C–C Single-Bond Cleavage of Alcohols. *Org. Lett.* **2021**, *23* (21), 8413–8418. c) Xiong, N.; Li, Y.; Zeng, R. Iron-Catalyzed Photoinduced Remote C(Sp3)–H Amination of Free Alcohols. *Org. Lett.* **2021**, *23* (22), 8968–8972. d) Xue, T.; Zhang, Z.; Zeng, R. Photoinduced Ligand-to-Metal Charge Transfer (LMCT) of Fe Alkoxide Enabled C–C Bond Cleavage and Amination of Unstrained Cyclic Alcohols. *Org. Lett.* **2022**, *24* (3), 977–982.

(13) For rare examples of arylations by dual catalysis involving Fe-LMCT, see: a) Zou, L.; Wang, X.; Xiang, S.; Zheng, W.; Lu, Q. Paired Oxidative and Reductive Catalysis: Breaking the Potential Barrier of Electrochemical C(sp^3)–H Alkenylation. *Angew. Chem. Int. Ed.* **2023**, *62* (24), e202301026. b) Xiong, N.; Li, Y.; Zeng, R. Merging Photoinduced Iron-Catalyzed Decarboxylation with Copper Catalysis for C–N and C–C Couplings. *ACS Catal.* **2023**, *13* (3), 1678–1685. c) Zou, L.; Xiang, S.; Sun, R.; Lu, Q. Selective C(sp^3)–H Arylation/Alkylation of Alkanes Enabled by Paired Electrocatalysis. *Nat. Commun* **2023**, *14* (1), 7992.

(14) During reviewing of this manuscript, two additional reports of dual catalysis involving Fe-LMCT appeared in the literature: a) Zou, L.; Sun, R.; Tao, Y.; Wang, X.; Zheng, X.; Lu, Q. Photoelectrochemical Fe/Ni cocatalyzed C–C functionalization of alcohols. *Nat. Commun.* **2024**, *15* (1), DOI: 10.1038/s41467-024-49557-7. b) Nsouli, R.; Nayak, S.; Balakrishnan, V.; Lin, J.-Y.; Chi, B. K.; Ford, H. G.; Tran, A.;

Guzei, I. A.; Bacsa, J.; Armada, N.; Zenov, F.; Weix, D. J.; Ackerman-Biegasiewicz, L. K. G. Decarboxylative Cross-Coupling Enabled by Fe and Ni Metallaphotoredox Catalysis. *ChemRxiv* **2024**, 10.26434/chemrxiv-2024-dmfhw.

(15) a) de Groot, L. H. M.; Ilic, A.; Schwarz, J.; Wärnmark, K. Iron Photoredox Catalysis–Past, Present, and Future. *J. Am. Chem. Soc.* **2023**, *145* (17), 9369–9388. b) Chen, J.; Browne, W. R. Photochemistry of Iron Complexes. *Coord. Chem. Rev.* **2018**, *374*, 15–35. c) Zhou, W.-J.; Wu, X.-D.; Miao, M.; Wang, Z.-H.; Chen, L.; Shan, S.-Y.; Cao, G.-M.; Yu, D.-G. Light Runs Across Iron Catalysts in Organic Transformations. *Chem. Eur. J.* **2020**, *26* (66), 15052–15064.

(16) Barreiro, E. J.; Kümmerle, A. E.; Fraga, C. A. M. The Methylation Effect in Medicinal Chemistry. *Chem. Rev.* **2011**, *111* (9), 5215–5246.

(17) For selected examples, see : a) Huihui, K. M. M.; Caputo, J. A.; Melchor, Z.; Olivares, A. M.; Spiewak, A. M.; Johnson, K. A.; DiBenedetto, T. A.; Kim, S.; Ackerman, L. K. G.; Weix, D. J. Decarboxylative Cross-Electrophile Coupling of N-Hydroxyphthalimide Esters with Aryl Iodides. *J. Am. Chem. Soc.* **2016**, *138* (15), 5016–5019. b) Zhang, P.; Le, C. "Chip"; MacMillan, D. W. C. Silyl Radical Activation of Alkyl Halides in Metallaphotoredox Catalysis: A Unique Pathway for Cross-Electrophile Coupling. *J. Am. Chem. Soc.* **2016**, *138* (26), 8084–8087. c) Kariofillis, S. K.; Shields, B. J.; Tekle-Smith, M. A.; Zacuto, M. J.; Doyle, A. G. Nickel/Photoredox-Catalyzed Methylation of (Hetero)Aryl Chlorides Using Trimethyl Orthoformate as a Methyl Radical Source. *J. Am. Chem. Soc.* **2020**, *142* (16), 7683–7689. d) Jin, J.; MacMillan, D. W. C. Alcohols as Alkylating Agents in Heteroarene C–H Functionalization. *Nature* **2015**, *525* (7567), 87–90. e) Chen, R.; Intermaggio, N. E.; Xie, J.; Rossi-Ashton, J. A.; Gould, C. A.; Martin, R. T.; Alcázar, J.; MacMillan, D. W. C. Alcohol-Alcohol Cross-Coupling Enabled by SH2 Radical Sorting. *Science* **2024**, *383* (6689), 1350–1357. f) He, Z.-T.; Li, H.; Haydl, A. M.; Whiteker, G. T.; Hartwig, J. F. Trimethylphosphate as a Methylating Agent for Cross Coupling: A Slow-Release Mechanism for the Methylation of Arylboronic Esters. *J. Am. Chem. Soc.* **2018**, *140* (49), 17197–17202. g) Heijnen, D.; Tosi, F.; Vila, C.; Stuart, M. C. A.; Elsinga, P. H.; Szymanski, W.; Feringa, B. L. Oxygen Activated, Palladium Nanoparticle Catalyzed, Ultrafast Cross-Coupling of Organolithium Reagents. *Angew. Chem. Int. Ed.* **2017**, *56* (12), 3354–3359. h) Vasilopoulos, A.; Krska, S. W.; Stahl, S. S. C(Sp3)–H Methylation Enabled by Peroxide Photosensitization and Ni-Mediated Radical Coupling. *Science* **2021**, *372* (6540), 398–403.

(18) Yuan, M.; Song, Z.; Badir, S. O.; Molander, G. A.; Gutierrez, O. On the Nature of C(sp^3)–C(sp^2) Bond Formation in Nickel-Catalyzed Tertiary Radical Cross-Couplings: A Case Study of Ni/Photoredox Catalytic Cross-Coupling of Alkyl Radicals and Aryl Halides. *J. Am. Chem. Soc.* **2020**, *142* (15), 7225–7234.

(19) Panzeri, G.; Accogli, A.; Gibertini, E.; Rinaldi, C.; Nobili, L.; Magagnin, L. Electrodeposition of high-purity nanostructured iron films from Fe(II) and Fe(III) non-aqueous solutions based on ethylene glycol. *Electrochimica Acta* **2018**, *271*, 576–581.

(20) Similar reactions were attempted with FeCl3 + 2 to 3 eq $\mathbf{L_{Fe9}}$ as well. Although precipitation of KCl and complete coordination of $\mathbf{L_{Fe9}}$ was witnessed as well, we failed to obtained X-Ray quality crystals from these mixtures.

(21) The presence of the central oxygen is surprising since the synthesis was performed in an N_2-filled glovebox using dried and degassed reagents. Its origin remains unknown at this stage.

(22) a) Cannon, R. D.; Montri, L.; Brown, D. B.; Marshall, K. M.; Elliott, C. M. Partial Electron Delocalization in a Mixed-Valence Trinuclear Iron(III)-Iron(II) Complex. *J. Am. Chem. Soc.* **1984**, *106* (9), 2591–2594. b) Overgaard, J.; Larsen, F. K.; Schiøtt, B.; Iversen, B. B. Electron Density Distributions of Redox Active Mixed Valence Carboxylate Bridged Trinuclear Iron Complexes. *J. Am. Chem. Soc.* **2003**, *125* (36), 11088–11099.

(23) Raya-Barón, Á.; Oña-Burgos, P.; Fernández, I. Diffusion NMR Spectroscopy Applied to Coordination and Organometallic Compounds. In *Annual Reports on NMR Spectroscopy*; Webb, G. A., Ed.; Academic Press, 2019; Vol. 98, pp 125–191.

(24) a) Poh, A. W. J.; Aguilar, J. A.; Kenwright, A. M.; Mason, K.; Parker, D. Aggregation of Rare Earth Coordination Complexes in Solution Studied by Paramagnetic and DOSY NMR. *Chem. Eur. J.* **2018**, *24* (60), 16170–16175. b) P. Crockett, M.; Zhang, H.; M. Thomas, C.; A. Byers, J. Adding Diffusion Ordered NMR Spectroscopy (DOSY) to the Arsenal for Characterizing Paramagnetic Complexes. *Chem. Commun.* **2019**, *55* (96), 14426–14429. c) Denis-Quanquin, S.; Riobé, F.; Delsuc, M.-A.; Maury, O.; Giraud, N. Paramagnetic DOSY: An Accurate Tool for the Analysis of the Supramolecular Interactions between Lanthanide Complexes and Proteins. *Chem. Eur. J.* **2016**, *22* (50), 18123–18131.

(25) a) An, Q.; Xing, Y.-Y.; Pu, R.; Jia, M.; Chen, Y.; Hu, A.; Zhang, S.-Q.; Yu, N.; Du, J.; Zhang, Y.; Chen, J.; Liu, W.; Hong, X.; Zuo, Z. Identification of Alkoxy Radicals as Hydrogen Atom Transfer Agents in Ce-Catalyzed C–H Functionalization. *J. Am. Chem. Soc.* **2023**, *145* (1), 359–376. b) Yang, Q.; Wang, Y.-H.; Qiao, Y.; Gau, M.; Carroll, P. J.; Walsh, P. J.; Schelter, E. J. Photocatalytic C–H Activation and the Subtle Role of Chlorine Radical Complexation in Reactivity. *Science* **2021**, *372* (6544), 847–852.

(26) a) Chrisman, C. H.; Kudisch, M.; Puffer, K. O.; Stewart, T. K.; Lamb, Y. M. L.; Lim, C.-H.; Escobar, R.; Thordarson, P.; Johannes, J. W.; Miyake, G. M. Halide Noninnocence and Direct Photoreduction of Ni(II) Enables Coupling of Aryl Chlorides in Dual Catalytic, Carbon–Heteroatom Bond-Forming Reactions. *J. Am. Chem. Soc.* **2023**, *145* (22), 12293–12304. (b) Vander Griend, D. A.; Bediako, D. K.; DeVries, M. J.; DeJong, N. A.; Heeringa, L. P. Detailed Spectroscopic, Thermodynamic, and Kinetic Characterization of Nickel(II) Complexes with 2,2'-Bipyridine and 1,10-Phenanthroline Attained via Equilibrium-Restricted Factor Analysis. *Inorg. Chem.* **2008**, *47* (2), 656–662.

(27) Neumeier, M.; Chakraborty, U.; Schaarschmidt, D.; de la Pena O'Shea, V.; Perez-Ruiz, R.; Jacobi von Wangelin, A. Combined Photoredox and Iron Catalysis for the Cyclotrimerization of Alkynes. *Angew. Chem. Int. Ed.* **2020**, *59* (32), 13473–13478.

(28) At this stage, we cannot exclude complexation of [Fe^{II}] by ROH first, followed by oxidation to [Fe^{III}-OR]

(29) Comproportionation with remaining Ni^{I} **E** is also possible. Reduction of the resulting $(\mathbf{L_{Ni8}})_m Ni^{II}X_2$ complex by $DPA^{-\bullet}$ would then turn over the cycle.

Graphical Abstract